



## Geometric Signatures of Jamming in the Mechanical Vacuum

Peter K. Morse and Eric I. Corwin

*Department of Physics and Materials Science Institute, University of Oregon, Eugene, Oregon 97403, USA*

(Received 16 October 2013; published 20 March 2014)

Jamming has traditionally been studied as a mechanical phenomenon and characterized with mechanical order parameters. However, this approach is not meaningful in the “mechanical vacuum” of systems below jamming in which all mechanical properties are precisely zero. We find that the network of nearest neighbors and the geometric structure of the Voronoi cell contain well-defined and meaningful order parameters for jamming, which exist on both sides of the transition. We observe critical exponents in these order parameters and an upper critical dimension of 3. Further, we present evidence for a new incipient-jamming phase below the jamming transition marked by additional symmetry in the Voronoi tessellation.

DOI: [10.1103/PhysRevLett.112.115701](https://doi.org/10.1103/PhysRevLett.112.115701)

PACS numbers: 64.70.-p, 45.70.-n, 61.43.Bn, 81.05.Kf

Since 1727 when the Reverend Stephen Hales studied the contact statistics of peas compressed in a pot [1], the study of jamming has primarily concerned itself with mechanical properties. It is well known how pressure [2], bulk and shear modulus [3–5], stress and strain [2], force [6], and contact number [7,8] scale with packing fraction  $\phi$  above the jamming point  $\phi_J$  [9]. While these properties can be used as order parameters to study the mechanical jamming transition, this understanding does not extend to the “mechanical vacuum.” The mechanical vacuum describes states below jamming wherein the system has no mechanical response and lacks stable force carrying contacts. This leaves half of the phase space with a trivial order parameter which does not capture the physical reality that a system slightly below jamming is very different from one far below jamming [10]. This phase space has previously been studied within the realm of liquid theory and hard-sphere jamming [11–14], but the structural properties of static unjammed packings have yet to be addressed.

High-dimensional sphere packings offer an opportunity to study the underlying physics and geometry of jamming [10,15,16]. Recent attempts to construct a field theory for jammed systems have been successful in describing mechanical properties. The Gaussian replica theory uses a mapping between spin glass systems and jammed systems to develop a field theory with predictive power for some scalings around jamming [13]. This theory is applicable in arbitrary dimensions and correctly predicts  $\phi_J$  will take on a range of values that are method dependent [16]. Recent simulational work has exploited finite-size scaling of the mechanical properties of jamming for  $d = 2$  and  $d = 3$  to find critical exponents and evidence for an upper critical dimension of  $d_{UCD} = 2$  [17]. However, because these works are restricted to mechanical properties, they cannot describe the physics of systems below jamming.

The local structure of jammed systems has also emerged as an active area of study. The properties of the nearest-neighbor network for sphere packings at and above

jamming are key components of granocentric models [18–22]. These models are purely local in scope and yet manage to predict global properties, suggesting that the local geometry plays an important role in jamming.

In this paper we analyze simulations of sphere packings using two local geometric quantities which are derived from the additively weighted Voronoi tessellation [23] of space around each particle: (1) the mean number of nearest neighbors and (2) the maximum inscribed sphere in each cell (Fig. 1). Both are well defined above and below jamming and, as will be shown, contain a signature of the jamming transition.

Packings of particles are created similarly to Refs. [16,24]. Particles exist in a  $d$ -dimensional hypercube with periodic

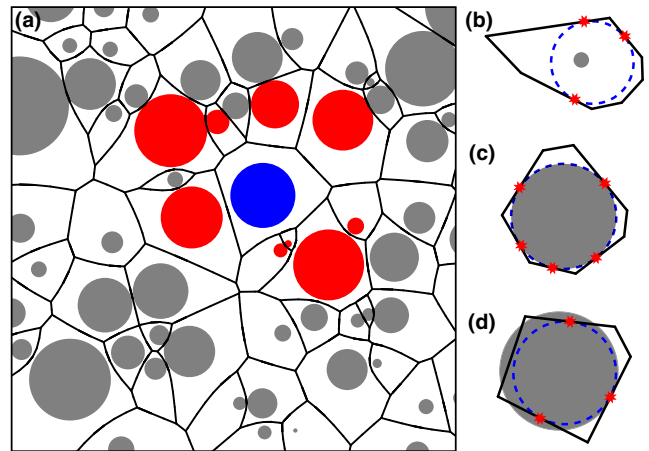


FIG. 1 (color online). (a) The additively weighted Voronoi tessellation for a polydisperse mixture of particles in two dimensions. The particle shown in blue has a set of nearest neighbors shown in red. (b-d) The maximum inscribed sphere (MIS) in a given Voronoi cell below jamming (b), at jamming (c), and above jamming (d). The physical particle is illustrated as a gray circle, the Voronoi cell is shown in black lines, the MIS is shown as a blue dashed circle, and the contacts between the MIS and the Voronoi cell are shown as red stars.

boundary conditions and unit side length and interact with a contact potential dependent on their dimensionless overlap,

$$\delta = 1 - \frac{\|\vec{x}_1 - \vec{x}_2\|}{r_1 + r_2}, \quad (1)$$

where  $\vec{x}_1$  and  $\vec{x}_2$  are the particle positions and  $r_1$  and  $r_2$  are the radii. The potential is defined as

$$V(\delta) = \begin{cases} \frac{\epsilon}{\alpha} \delta^\alpha & : \delta > 0 \\ 0 & : \delta \leq 0 \end{cases}, \quad (2)$$

where  $\alpha$  is the order of the potential ( $\alpha = 2$  for a Hookean potential and 2.5 for a Hertzian potential) and  $\epsilon$  is the characteristic energy scale chosen to be 1. Unless specified, we use  $\alpha = 2$ . A packing is considered unjammed if the energy of overlap per particle is less than  $10^{-20}$ .

We explore a wide range of packing fractions using two protocols: (1) infinite temperature quench (IQ) and (2) golden mean search (GM). The IQ protocol is used to create a packing at a specified  $\phi$  by placing particles randomly throughout the simulation volume with appropriately scaled radii [7]. The system is then relaxed to its local energy minimum using a home-built, GPGPU-optimized version of conjugate gradient minimization [25] or the fast inertial relaxation engine (FIRE) [26] running on the University of Oregon's ACISS supercomputer. We demonstrate in Supplemental Material Figs. 1 and 2 [27] that our results close to jamming are robust to choices among our minimization techniques. The GM protocol is used to approach arbitrarily close to the jamming point,  $\phi_J$ . The resulting value of  $\phi_J$  is dependent on whether jamming is approached from below or above, but the properties of packings at the transition do not depend on the packing history [16]. A GM packing is created from above (below) by choosing two packing fractions that bound  $\phi_J$ . An initial packing is created at the bound above (below) using the IQ protocol. The radii of particles in this packing are then scaled by a uniform factor to achieve an intermediate packing fraction and re-minimized. If the resulting packing remains above (below) jamming it is made the new upper (lower) bound and the process continues. If it is below (above) then it becomes the new lower (upper) bound and a new packing is made by dilating the previous upper (lower) bound packing. This process is continued until the upper and lower bounds differ by less than 1 part in  $10^{15}$ .

The nearest-neighbor network determines the local environment of a particle. For a given particle, the additively weighted Voronoi (sometimes called the navigation map or Johnson-Mehl tessellation) cell contains all points in space closer to the particle's surface than to that of any other particle [23]. For monodisperse particles this reduces to the Voronoi diagram in which all cells have flat interfaces. Two particles are said to be nearest neighbors if their respective cells share an interface. In order to

calculate the additively weighted Voronoi tessellation in high dimensions, we implemented the algorithm described by Boissonnat and Delage [28]. However, we should note that our results continue to hold for other choices of tessellation, most notably the radical Voronoi (or Laguerre) tessellation, as demonstrated in Supplemental Material Fig. 3 [27]. As a packing approaches jamming, the neighbor network is very sensitive to the small spatial rearrangements of particles. We observe a continuous phase transition in the mean number of neighbors  $\langle N \rangle$  as a function of packing fraction [Fig. 2(a)]. All curves for dimensions  $d \geq 3$  collapse onto a single master curve near  $\phi_J$  when scaled as  $(\langle N \rangle - N_J)/kN_J$  vs  $(\phi - \phi_J)/\phi_J$ , where  $k$  is a tunable parameter of order 1 and  $N_J$  is the mean number of nearest neighbors at jamming and  $\phi_J$  is the

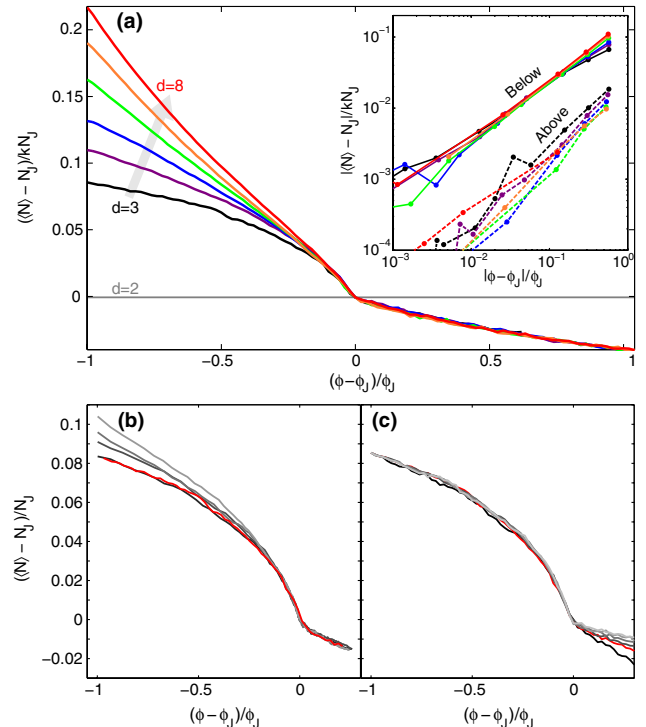


FIG. 2 (color online). (a) The scaled mean number of neighbors as a function of scaled distance to the jamming point. Shown are  $d = 2$  (gray), 3 (black), 4 (purple), 5 (blue), 6 (green), 7 (orange), 8 (red). The  $k$  values used for collapse are 1, 1, 1.4, 1.4, 1.2, 1, and 0.75, respectively. All packings are created using the infinite temperature quench (IQ) protocol. Inset, log-log plot of scaled mean number of neighbors as a function of distance to the jamming point for  $d \geq 3$ . Packings plotted in the inset are created using the GM protocol from below the jamming transition (solid lines) and above (dashed lines). (b) Scaled mean neighbor number for varied polydispersity in  $d = 3$ . The radii of the polydisperse particles are drawn from a log-normal distribution with  $\mu = 1$  and  $\sigma$  ranging from 0 (red), 0.05 (black) up to 0.2 (light gray) in steps of 0.05. (c) Scaled mean neighbor number for varied power-law potentials. Values of the order of the potential  $\alpha$  range from 1.5 (black) to 4 (light gray) with the Hookean potential ( $\alpha = 2$ ) shown in red.

TABLE I. Table of  $\langle N \rangle$  at zero density for dimensions 1–8.

| d                   | 1 | 2 | 3                  | 4     | 5       | 6       | 7       | 8        |
|---------------------|---|---|--------------------|-------|---------|---------|---------|----------|
| $\langle N \rangle$ | 2 | 6 | $(48\pi^2/35) + 2$ | 340/9 | 89.3(8) | 203.(6) | 458.(8) | 1016.(3) |

jamming density found through our GM protocol. Note that  $k$  is a scale factor which only depends on dimension, similar to the universal amplitude ratio of the lambda transition [29]. This master curve has power-law scaling on both sides of the transition point with exponents  $\approx 0.75$  as shown in the inset to Fig. 2(a), demonstrating that  $\phi_J$  controls the physics on both sides of the transition. There is no *a priori* reason why the power laws on either side should be the same or different and our data is insufficient to conclusively distinguish the two. For  $d = 2$  this curve is trivially flat due to the Euler relation which requires  $\langle N \rangle = 6$  for all  $\phi$  [30]. Since this collapse only occurs for  $d \geq 3$ , we have evidence for an upper critical dimension of  $d_{\text{UCD}} = 3$ , in stark contrast to the mechanical picture which yields  $d_{\text{UCD}} = 2$  [2,17].

Individual curves peel away from the master curve in Fig. 2(a) when sufficiently far below  $\phi_J$ . There is a seemingly trivial point in phase space at  $\phi = 0$  which nonetheless controls the physics of low-density packings. At zero density the contact potential and polydispersity are meaningless as every particle has radius  $r = 0$  and zero overlap. The network of nearest neighbors at this point is thus the result of a Poisson process and its properties are calculable using stochastic geometry [31,32]. Analytic values for  $\langle N \rangle$  at zero density have been found for  $d \leq 4$  [32] and agree with our results to within numerical error. Exact values have not yet been derived in higher dimensions but are easily numerically computed with our simulations (Table I). Systems very close to zero density are controlled by this point up to a cross-over density, beyond which the system is controlled by  $\phi_J$ .

The effect of sample polydispersity is shown in Fig. 2(b). Varying polydispersity changes the numerical value of  $\phi_J$  [33], but the shape of the curve near jamming is unchanged. This suggests that the distance between surfaces of particles is more important to the dynamics of the phase transition than center-to-center distance. Thus, monodisperse and polydisperse packings are controlled by the same physics in this regime.

Figure 2(c) demonstrates the effect of varying the contact potential. We use power law contact potentials [Eq. (2)] with order  $\alpha$  ranging from 1.5 to 4. All potentials follow the same master curve below jamming. This is unsurprising because below jamming the only role of the potential is to prevent overlap. Above jamming, the potential determines the distribution of overlaps between particles which in turn determines the local structure of the packing. This is manifested by a change in the slope of the curve above  $\phi_J$  with lower order potentials giving steeper slopes, suggesting

that higher order potentials tend to lock in local structure and give higher barriers to structural rearrangements.

The maximum inscribed sphere (MIS) in the Voronoi cell of each particle contains a very different signature of the jamming transition. The radius  $R$  of the MIS in a given Voronoi cell is calculated using an algorithm similar to the FIRE minimization of particle packings and an imposed repulsive harmonic potential between the inscribed sphere and the cell walls. We perform a GM search by choosing two radii that bound the true MIS radius. If the minimized energy is less than  $10^{-20}$ , the test radius is now used as the lower bound, and if it is greater, the test radius is used as the upper bound. The search process is continued until the upper and lower bounds differ by less than 1 part in  $10^{15}$ .

Figure 3(a) shows  $P(r - R/L)$ , the distribution of the normalized difference between the MIS radii,  $R$ , and the particle radius,  $r$ , for monodisperse particles in  $d = 3$ . We normalize the difference in radii by the characteristic distance between centers  $L = \rho^{-d}$  where  $\rho$  is the number density of particles. Below jamming no particles overlap; therefore, the MIS radius  $R$  must be strictly less than the particle radius  $r$  [Fig. 1(b)]. Above jamming every non-rattler particle has some overlap; therefore the MIS radius  $R$  must be strictly greater than the particle radius  $r$  [Fig. 1(d)]. At jamming the particle is fully constrained and kissing the boundaries of the Voronoi cell [Fig. 1(c)] causing the MIS to be identical to the particle. Therefore, any translation or dilation relative to the jammed particle must puncture the surface of the Voronoi cell. Thus, at jamming  $P(r - R/L)$  must be a  $\delta$  function at zero. In this way jamming links the mechanical structure of a packing to the geometric structure of the nearest-neighbor network.

Because the functional form of the MIS distribution changes dramatically, and to discount the influence of rattlers, we characterize its evolution with packing fraction by defining a distribution width  $\Delta R/r$  to be the width of the middle 80% of the distribution. We use this definition of width rather than the standard deviation to minimize the influence of rattlers. We find that our width is robust to changes in this cutoff value (Supplemental Material Fig. 4 [27]). When we approach jamming from above [the right side of Fig. 3(b)] we see a linear convergence to zero in  $\Delta R/r$  at  $\phi_J$  [Fig. 3(d)]. However, when we approach from below jamming [left side of Fig. 3(b)], we also see a convergence of the width toward zero but at a packing fraction significantly less than  $\phi_J$ . We call this new critical point  $\phi^*$  and find that  $\Delta R/r$  approaches this point from below with a power law of  $\approx 2$  [Fig. 3(c) inset and tabulated in Supplemental Material Fig. 5 [27]].

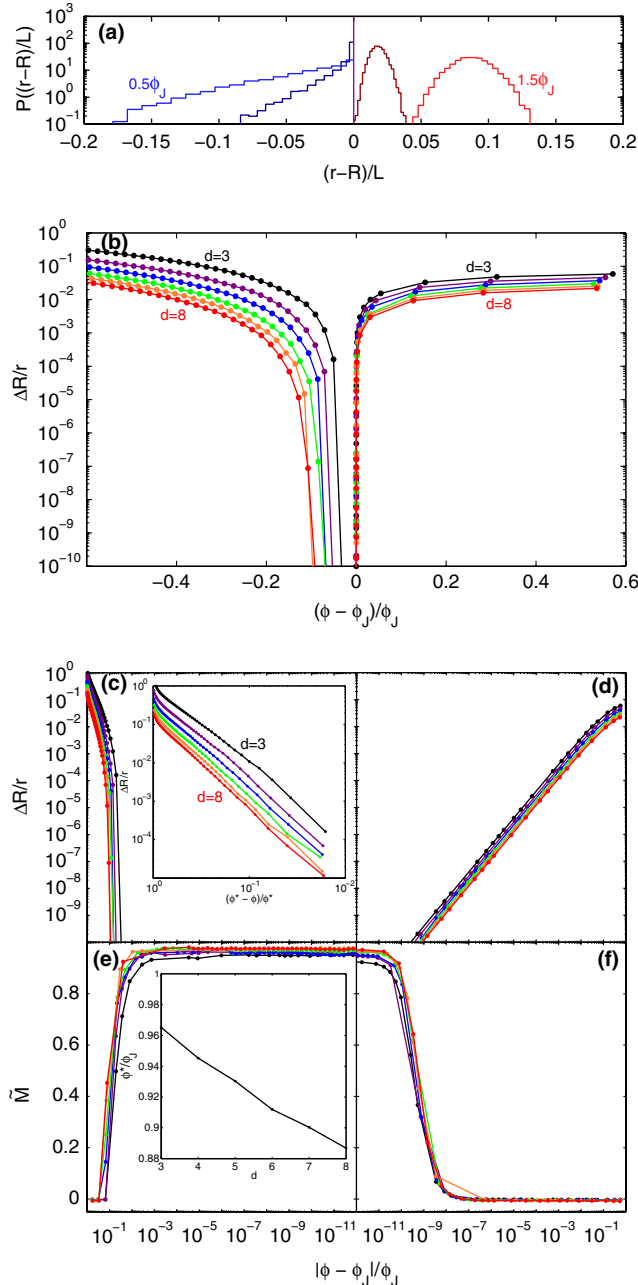


FIG. 3 (color online). (a) Distributions of radii of MIS at  $0.5\phi_J$  (light blue),  $0.9\phi_J$  (dark blue),  $\phi_J$  (purple),  $1.1\phi_J$  (dark red), and  $1.5\phi_J$  (light red) for  $d = 3$ . The packings above and below jamming were made using the IQ protocol, and the jammed packing was made using the GM protocol from above. (b) Semilog plot of scaled distribution width of MIS as a function of scaled distance to the jamming transition. The color scheme is the same as in Fig. 2(a). (c) Log-log plot of scaled distribution width for packings approaching jamming from below with GM protocol. Inset, power-law behavior shows  $\Delta R/r$  approaching  $\phi^*$  quadratically. (d) Log-log plot of scaled distribution width for packings approaching jamming from above showing a power-law with exponent 1. (e)–(f) Plot of the scaled number of constraints on the MIS as a function of scaled distance to the jamming point. Packings are created using the GM protocol. Inset, plot of  $\phi^*/\phi_J$  as a function of dimension  $d$ .

As a consequence of the identity between the particle and the MIS at jamming the mean number of constraints  $\langle M \rangle$  on the MIS should also contain a signature of jamming. In general, the MIS in a convex polytope in  $d$  dimensions is constrained to contact  $M = d + 1$  sides of the cell. However, since jammed packings at  $\phi_J$  are mechanically stable they satisfy isostaticity, which requires the mean number of contacts  $\langle Z \rangle = 2d$  [17]. This in turn requires that the mean number of constraints on the MIS be  $M = 2d$ . In order for an inscribed sphere to have more than  $d + 1$  contacts there must be degeneracy in the constraints. This implies that a heretofore unobserved symmetry must be present in the Voronoi cells at jamming.

We define the normalized number of constraints  $\tilde{M}$  on an MIS as

$$\tilde{M} = \frac{M - (d + 1)}{2d - (d + 1)}, \quad (3)$$

such that at jamming where  $M = 2d$ ,  $\tilde{M} = 1$  and generically when  $M = d + 1$ ,  $\tilde{M} = 0$ . As expected, we see a transition in  $\tilde{M}$  from  $\tilde{M} = 0$  far from jamming to  $\tilde{M} = 1$  close to jamming. When approaching jamming from above the transition happens at a distance to  $\phi_J$  comparable to our numerical precision [Fig. 3(f)], whereas when approaching from below the transition occurs at  $\phi^*$  rather than at  $\phi_J$  [Fig. 3(e)]. This is further evidence that  $\phi^*$  is a meaningful critical point related to this new symmetry. The ratio  $\phi^*/\phi_J$  decreases linearly with increasing dimension, indicating that the phase between  $\phi^*$  and  $\phi_J$  becomes more important in higher dimensions [Fig. 3(e) inset].

Our results demonstrate that the geometric structure of a packing contains a clear signature of the jamming transition. We have measured critical exponents in order parameters derived from this geometric structure which should prove instrumental to developing a fully realized field theory for both sides of the jamming transition. Surprisingly, we find  $d_{\text{UCD}} = 3$  whereas measures of mechanical properties yield  $d_{\text{UCD}} = 2$ . This result can be interpreted in one of two alternative ways. Either (1) there are two independent phase transitions, one mechanical and the other geometric, that happen to coincide at precisely the same point in phase space, or (2) the jamming-unjamming transition is a new type of phase transition consisting of linked mechanical and geometric transition with different  $d_{\text{UCD}}$ . Each interpretation is unsettling in its own way. It beggars belief that two entirely independent phase transitions would just happen to precisely coincide, so (1) seems quite unlikely. Interpretation (2) requires the extraordinary claim that the jamming transition is characteristically unlike any other understood physical process. Indeed, jamming and by extension the glass transition [34] has been curiously resistant to theoretical explanation. Under either interpretation these results point the way towards new physics.

Finally, we observe a new critical point  $\phi^*$  well below  $\phi_J$ . This new critical point is obscured by the mechanical vacuum, and there is no signature of it in simple statistics of the neighbor network. One can only find it by looking at the local structure of Voronoi cells. It remains to be uncovered what underlying symmetry is revealed by this phase transition.

We thank John Toner for helpful discussions. We thank the NSF for support under CAREER Award No. DMR-1255370 and GK12 No. DGE-0742540. The ACISS supercomputer is supported under a Major Research Instrumentation Grant, Office of Cyber Infrastructure, No. OCI-0960354.

- 
- [1] S. Hales, W. J. Innys, and T. Woodward, *Statistical Essays: Vegetable Statics* (Royal Academy, London, UK, 1727).
- [2] C. S. O'Hern, L. E. Silbert, A. J. Liu, and S. R. Nagel, *Phys. Rev. E* **68**, 011306 (2003).
- [3] M. Wyart, *Ann. Phys. (Berlin)* **30**, 1 (2005).
- [4] W. G. Ellenbroek, E. Somfai, M. van Hecke, and W. van Saarloos, *Phys. Rev. Lett.* **97**, 258001 (2006).
- [5] B. P. Tighe, E. Woldhuis, J. J. C. Remmers, W. van Saarloos, and M. van Hecke, *Phys. Rev. Lett.* **105**, 088303 (2010).
- [6] C. S. O'Hern, S. A. Langer, A. J. Liu, and S. R. Nagel, *Phys. Rev. Lett.* **86**, 111 (2001).
- [7] C. S. O'Hern, S. A. Langer, A. J. Liu, and S. R. Nagel, *Phys. Rev. Lett.* **88**, 075507 (2002).
- [8] B. P. Tighe, *Phys. Rev. Lett.* **109**, 168303 (2012).
- [9] M. v. Hecke, *J. Phys. Condens. Matter* **22**, 033101 (2010).
- [10] M. Skoge, A. Donev, F. H. Stillinger, and S. Torquato, *Phys. Rev. E* **74**, 041127 (2006).
- [11] Z. W. Salsburg and W. W. Wood, *J. Chem. Phys.* **37**, 798 (1962).
- [12] A. Donev, F. H. Stillinger, and S. Torquato, *Phys. Rev. Lett.* **95**, 090604 (2005).
- [13] G. Parisi and F. Zamponi, *Rev. Mod. Phys.* **82**, 789 (2010).
- [14] W. Kob and L. Berthier, *Phys. Rev. Lett.* **110**, 245702 (2013).
- [15] P. Charbonneau, A. Ikeda, G. Parisi, and F. Zamponi, *Phys. Rev. Lett.* **107**, 185702 (2011).
- [16] P. Charbonneau, E. I. Corwin, G. Parisi, and F. Zamponi, *Phys. Rev. Lett.* **109**, 205501 (2012).
- [17] C. P. Goodrich, A. J. Liu, and S. R. Nagel, *Phys. Rev. Lett.* **109**, 095704 (2012).
- [18] J. A. Dodds, *Nature (London)* **256**, 187 (1975).
- [19] M. Clusel, E. I. Corwin, A. O. N. Siemens, and J. Brujić, *Nature (London)* **460**, 611 (2009).
- [20] J. G. Puckett, F. Lechenault, and K. E. Daniels, *Phys. Rev. E* **83**, 041301 (2011).
- [21] K. A. Newhall, I. Jorjadze, E. Vanden-Eijnden, and J. Brujic, *Soft Matter* **7**, 11518 (2011).
- [22] C. B. O'Donovan, E. I. Corwin, and M. E. Möbius, *Philos. Mag.* **93**, 4030 (2013).
- [23] F. P. Preparata and M. I. Shamos, *Computational Geometry: An Introduction*. (Springer, Berlin, 1985).
- [24] E. I. Corwin, R. Stinchcombe, and M. F. Thorpe, *Phys. Rev. E* **88**, 014102 (2013).
- [25] M. R. Hestenes and E. Stiefel, *J. Res. Natl. Bur. Stand.* **49**, 409 (1952).
- [26] E. Bitzek, P. Koskinen, F. Gähler, M. Moseler, and P. Gumbsch, *Phys. Rev. Lett.* **97**, 170201 (2006).
- [27] See Supplemental Material at <http://link.aps.org/supplemental/10.1103/PhysRevLett.112.115701> for comparisons between various packing protocols, a comparison between radical Voronoi and additively weighted Voronoi for polydisperse packings, and various distribution widths used for the maximum inscribed sphere radius. The figures highlight the robustness of our model. The supplement also contains numerical values for  $\phi_J$  and  $\phi^*$ .
- [28] J.-D. Boissonnat and C. Delage, in *Algorithms—ESA 2005*, edited by D. Hutchison *et al.* (Springer, Berlin, 2005), Vol. 3669, p. 367.
- [29] V. Privman, P. Hohenberg, and A. Aharony, *Phase Transitions and Critical Phenomena*, edited by C. Domb and J. Lebowitz (Academic, New York, 1991), Vol. 14.
- [30] L. Euler, *Novi Commentarii Academiae Scientiarum Imperialis Petropolitanae* Vol. 14, 109 (Typis Academiae Scientiarum, Petropoli, 1758).
- [31] J. L. Meijering, *Philips Res. Rep.* **8**, 270 (1953).
- [32] J. Møller, *Adv. Appl. Probab.* **21**, 37 (1989).
- [33] R. S. Farr and R. D. Groot, *J. Chem. Phys.* **131**, 244104 (2009).
- [34] A. J. Liu and S. R. Nagel, *Nature (London)* **396**, 21 (1998).